Materials Science and Engineering A 532 (2012) 111–119

Contents lists available at SciVerse ScienceDirect

Materials Science and Engineering A

journal homepage: www.elsevier.com/locate/msea

Adiabatic shear banding in AISI 1045 steel during high speed machining: Mechanisms of microstructural evolution

C.Z. Duan[1], L.C. Zhang*

School of Mechanical and Manufacturing Engineering, The University of New South Wales, NSW 2052, Australia

ARTICLE INFO

Article history:
Received 15 August 2011
Received in revised form 11 October 2011
Accepted 15 October 2011
Available online 25 October 2011

Keywords:
High speed machining
Adiabatic shear band
Microstructure evolution
Recrystallization
Serrated chip
Equiaxed grains
Subgrain
Grain reorientation

ABSTRACT

This paper presents an in-depth investigation into the formation mechanisms and microstructures of adiabatic shear bands (ASBs) in hardened AISI 1045 steel induced by high speed machining (HSM). A systematic analysis, both experimentally and theoretically, shows that a low cutting speed leads to deformed ASBs, and a high cutting speed results in transformed ASBs. The formation mechanisms of the two types of ASBs are fundamentally different. A deformed ASB is simply due to severe plastic shear, but a transformed ASB involves a process of reorientation and elongation of the martensite laths in the hardened steel, and the partitioning of elongated subgrains. It was found that a dynamic rotational recrystallization is likely the origin of the equiaxed grains in the center of a transformed ASB.

1. Introduction

High speed machining (HSM) has many advantages such as its high productivity and good quality in surface finish. As such, HSM has recently been used in aircraft, aerospace, automotive, die/mould-making and defense industries. However, it has been found that the serrated chipping associated with HSM has a significant influence on the cutting force, cutting temperature, tool wear, and surface integrity of the machined elements. Experiments have shown that in the primary shear zones of a serrated chip, adiabatic shear bands (ASBs) appear. The studies have concluded that it is the ASBs that make the serrated chipping.

In mechanical terms, an adiabatic shear is the result of thermal–mechanical instability in a material, localized in an extremely narrow band, when thermal-softening exceeds strain hardening. This phenomenon has been often observed in the deformation of materials subjected to various high-strain-rate conditions such as ballistic impact [1–5], explosive fragmentation [6–10], dynamic compression [11–17] and torsion [18], rolling [19,20] and welding [21]. These materials include steel [3,5,7,10,13,14,20], aluminum alloys [4,6], magnesium alloys [1,20,21], tantalum alloys [16], copper [17], titanium alloys [2,8,9,11,12] and Ni-based alloys [18]. Two types of ASBs have been reported based on optical microscopy studies, i.e., the '*deformed shear bands*' and the '*transformed shear bands*' [22–24], of which the former is caused by large plastic deformation and the latter, as the name stands, is associated with microstructural changes. The transformed shear bands are also called the '*white-etching bands*' sometimes, because of their 'white' color due to the formation of fine grains in ASBs, although such color-based justification is inaccurate. Recent studies have found that the formation of various microstructures in ASBs depends on materials and deformation processes [22]. The investigations have also reported that ASBs can have a broad range of microstructural alterations, such as recrystallization, phase transformation and amorphization [24].

To reveal the formation mechanism of ASBs in high speed machining, a thorough microstructural analysis under electron microscopy is important. Nevertheless, due to the difficulties in specimen preparations (particularly those for TEM analysis), very few investigations on the microstructures of ASBs in serrated chips have been conducted. Duan et al. [25–27] studied the microstructures in the ASBs of HSM chips of high strength steels using SEM and TEM, and found that the transformed bands contained equiaxed grains of about 0.1 μm in diameter. They suggested that the recrystallization and phase transformation could be simultaneous during the formation of the ASBs. Puerta Velasquez et al. [28]

* Corresponding author. Tel.: +61 2 9385 6078; fax: +61 2 9385 7316.
E-mail address: liangchi.zhang@unsw.edu.au (L.C. Zhang).
[1] On leave from the School of Mechanical Engineering, Dalian University of Technology, 116024, PR China.

0921-5093/$ – see front matter © 2011 Elsevier B.V. All rights reserved.
doi:10.1016/j.msea.2011.10.071

analysed the HSM chips of the Ti_6Al_4V alloy using SEM and EBSD, but concluded that no phase transformation took place in the ASBs, although they did not investigate the details of the microstructure. Some studies reported that the shiny zone in the ASBs of various steels could be re-crystallized fine structures with an associated dissolution of carbides, resulting in an increased resistance to etching [29]. These features were roughly defined as phase transformation products. In the formation of ASBs in HSM, the thermo-mechanical deformation of a metal involves large strain, high strain rate and very localized heating. The process is so complex that many fundamentals, such as the following, remain open:

(1) What is the microstructural evolution process in an ASB generated during HSM?
(2) What is the mechanism of re-crystallization, if any?

This paper aims to answer these questions. To explore the metallurgical details of individual microstructural zones in the ASBs of a serrated chip, the microstructural evolution leading to the ASBs will be characterized.

2. Experimental

2.1. Machining setup

AISI 1045 steel was used in this study. A steel ingot before heat treatment was machined into a cylindrical tube workpiece with its external diameter of ∅153 mm and wall thickness of 2.5 mm. A heat treatment was then conducted under the following conditions and procedures: heating the workpiece to 850 °C in vacuum and maintaining this temperature for 70 min; then quenching it in salt water, followed by a tempering at 360 °C for 5 h. The obtained hardness of the workpieces was HRC 50. The cutting tool was a carbide blade, YT15. The HSM was conducted as dry turning on lathe CA6140. In order to keep the sharpness of the cutting tool noses, the cutting tool inserts were replaced as required during the experiment. The cutting conditions used were: cutting speed v = 48–538 m/min, depth of cut a_c = 0.15 mm and tool rake angle $\gamma_0 = -10^\circ$. The cutting and thrust forces, F_c and F_T, were measured by a piezoelectric dynamometer.

2.2. Chip sample preparation for microscopy analysis

A collected chip was first set into the bakelite powder horizontally with a side surface on top to expose its sawteeth. After grinding, polishing and eroding, the morphology and microstructure of the chip were examined under a Neuphot-II optical microscope and JSM-5600LV SEM to allow measuring the height of the chip and its sawteeth, the separation angles between the shear band and the bottom of the chip, and the shear band width.

The chip specimens for TEM analysis must be prepared separately for examining the microstructures of the ASBs. Because a chip is very thin, it is difficult to handle and allocate its side surfaces. Thus before thinning a chip down, its top and bottom surfaces (see the illustration in Fig. 1) were first electroplated by Nickel to a certain thickness to make the specimen manageable. The specimens were then glued to a flat metal plate for grinding and polishing to a thickness of about 50 μm. The ASB zones in the chips were further thinned down by focused ion beam milling to a thickness suitable for TEM analysis. The microstructural examinations in ASBs were done on at least 3 samples to ensure the reliability of the results. The examinations were performed on an H-800 analytical TEM, operated at 200 kV with $L\lambda$ = 24.33 mm Å.

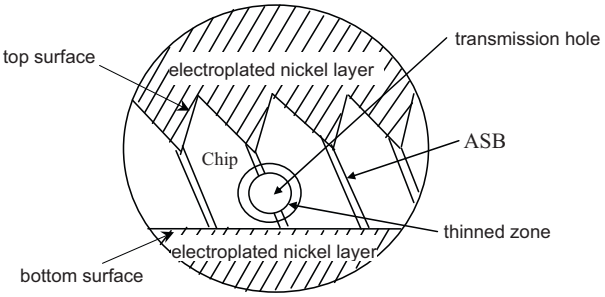

Fig. 1. Sketch map of preparation for TEM film sample of sawtooth chip.

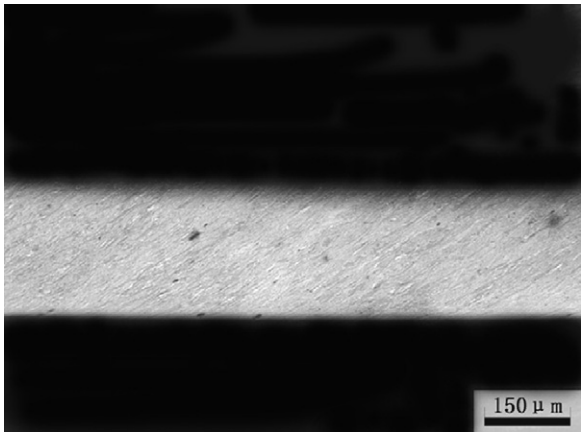

Fig. 2. An optical image of a ribbon chip (cutting speed v = 46.2 m/min).

3. Results and discussion

3.1. Microstructural analysis

Fig. 2 shows a smooth ribbon chip produced at a low cutting speed, 46.2 m/min. The entire chip thickness is relatively uniform. The chip deformation is in the form of homogeneous glide. No deformation localization was observed. Figs. 3 and 4 show that as the cutting speed increases (240.3 m/min and 432.6 m/min), serrated chipping took place. ASBs appear regularly in the primary shear zones between the sawteeth. The ASBs are of two types based on their different microstructural features. One of them (Fig. 3) has a highly localized straining zone with a width of about 50 μm. In this zone, however, the material has shown no sign of a phase change,

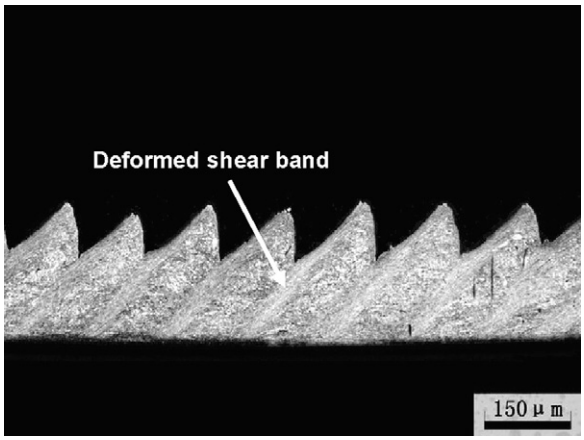

Fig. 3. An optical image of a serrated chip with deformed shear bands (cutting speed v = 240.3 m/min).

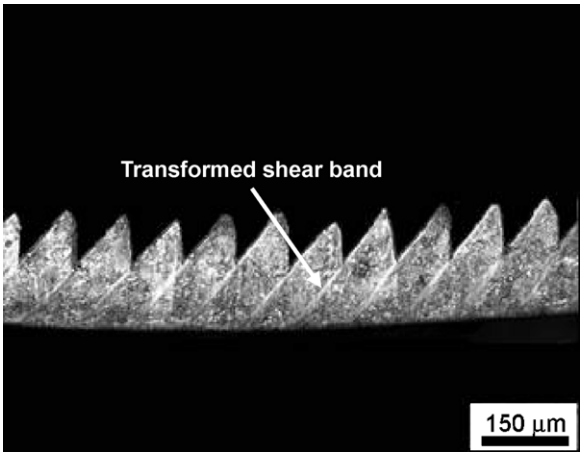

Fig. 4. An optical image of a serrated chip with transformed shear bands (cutting speed v = 432.6 m/min).

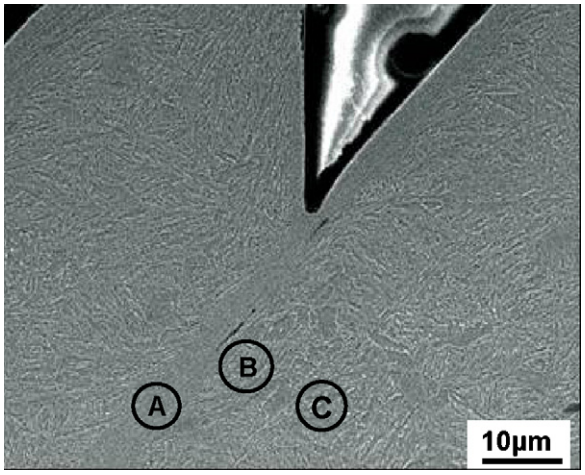

Fig. 6. An SEM image of a transformed shear band (cutting speed v = 432.6 m/min).

but has experienced severe plastic shear with a high density of slip lines. Therefore, this type of ASBs is the deformed shear bands. The second type of the ASBs observed (Fig. 4), of about 10 μm in width, show bright, smooth and white bands of morphology after erosion. The materials within the bands have distinct characteristics of a microstructural change during the adiabatic temperature rise. These are therefore the transformed shear bands. It is worth noting that the deformed shear bands formed under lower cutting speeds (e.g., v = 240.3 m/min), but the transformed shear bands emerged under higher cutting speeds (e.g., v = 432.6 m/min), indicating that the deformed and transformed shear bands occurred under different strain rates when the other cutting conditions are the same.

Figs. 5 and 6 are the SEM micrographs showing the details of the ASBs in Figs. 3 and 4, respectively. In Fig. 5, it can be seen that there is not a clear boundary between the deformed band and the surrounding material. The microstructure in the ASB was clearly elongated along the shear direction, indicating that the material in the deformed band had experienced a large plastic deformation. Approaching the center of ASB, the glide lines become denser. This suggests that the deformation in the center is much severer. The formation mechanism of such microstructures can be described as follows. Due to the high strain hardening effect, a great number of mobile dislocations were initiated and accumulated during the HSM in the primary shear zone to produce the deformed bands. As a result, the deformed band contains elongated and broken microstructures, but without a phase change because at a low cutting speed the local adiabatic temperature rise is insufficient.

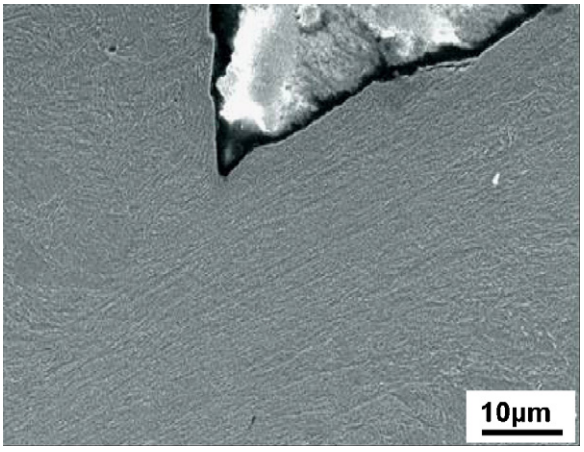

Fig. 5. An SEM image of a deformed shear band (cutting speed v = 240.3 m/min).

However, a transformed shear band (Fig. 6) has a well-defined width of distinct boundaries, indicating a different formation mechanism from that of a deformed band. An important feature is that the microstructure change from the band center to the surrounding chip material can be divided into three obvious zones, say *A*, *B* and *C*, as denoted in Fig. 6, where *A* represents the central zone of the band, *C* is the surrounding chip material, and *B* is the transitional zone from *A* to *C*. It is clear that the chip material (i.e., the material in zone *C*) experienced very little deformation and keeps almost its original structure. In the transitional zone *B*, the grains were elongated along the shear direction, which is similar to the characteristic in the deformed band mentioned above, and imply that the microstructure in the transitional zone can be an intermediate stage during the sequence of microstructural rearrangements leading to the transformed band. In the central zone *A*, the microstructure of the material becomes very different, showing very fine non-deformed structures as the result of localized sever shear and grain refinement.

To further explore the details of the microstructures, we carried out a series of TEM analysis. Fig. 7(a) shows the more detailed microstructure at the center of the deformed band. It can be seen that the martensite laths were elongated along the shear direction and were broken. There are dense dislocations between the laths. Fig. 7(b) shows the regular diffraction pattern of [1 1 1] zone axis of martensite, without any austenite diffraction spots. These indicate that the deformed shear band contains broken, tempered martensite due to large plastic shear. The temperature rise in the band had not exceeded the recrystallization or austenitization temperature; thus no recovery, recrystallization or phase transformation took place.

Fig. 8 shows the TEM images of the materials in zone *C* of Fig. 6. The original martensite laths are confirmed by the bright field image as seen in Fig. 8(a). The corresponding diffraction pattern in Fig. 8(b) shows a regular diffraction lattice of [1 1 1] zone axis of the martensite. Dislocations distribute inside and between the laths. A few twins also appear within the laths. These demonstrate that dislocation slipping was the main mechanism of plastic deformation because of the relatively lower strain and strain rate levels that the materials in this zone had experienced. Hence, the original morphology of the martensite lath in this zone was retained.

Figs. 9 and 10 show the microstructures of the materials in the transitional zone *B* in a transformed shear band. Fig. 9(a) displays the lath structure of the material at a point away from the band center. It can be seen that these laths are intensely elongated along the

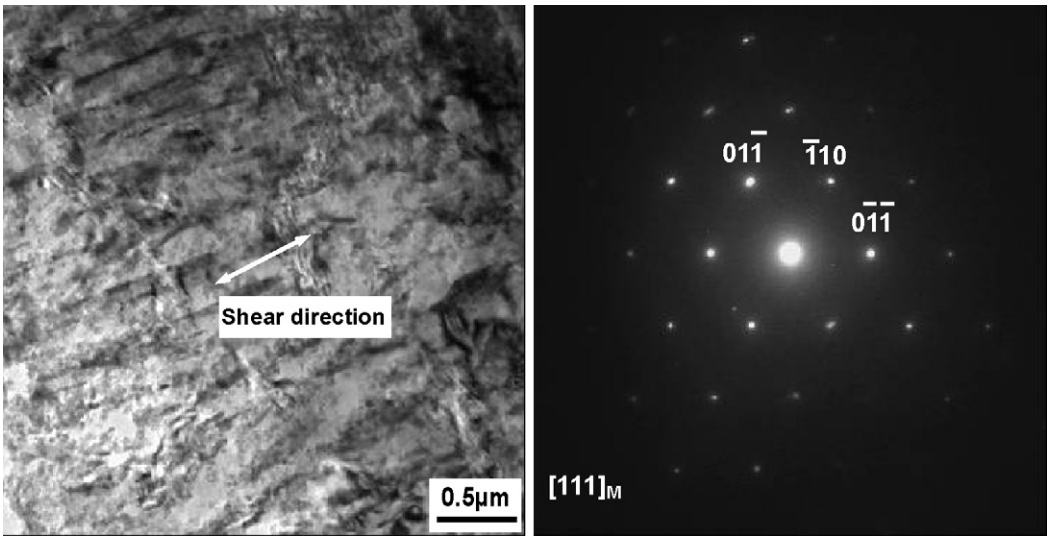

Fig. 7. TEM images of a deformed shear band. (a) The bright field image showing the broken and elongated martensite laths, and (b) the corresponding SAED pattern.

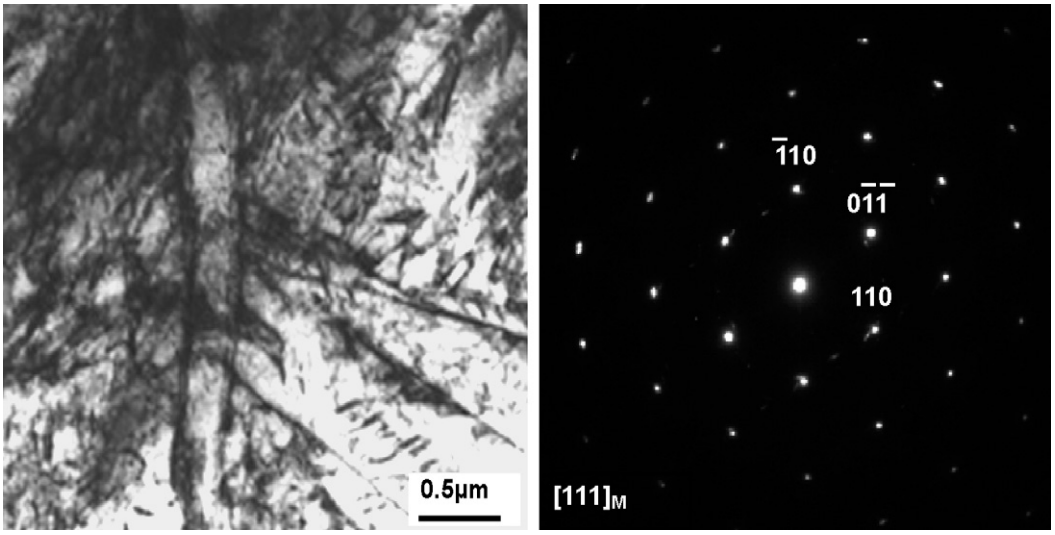

Fig. 8. TEM images of surrounding chip material *C* near the transformed shear band. (a) The bright field image showing the common martensite laths, and (b) the corresponding SAED pattern.

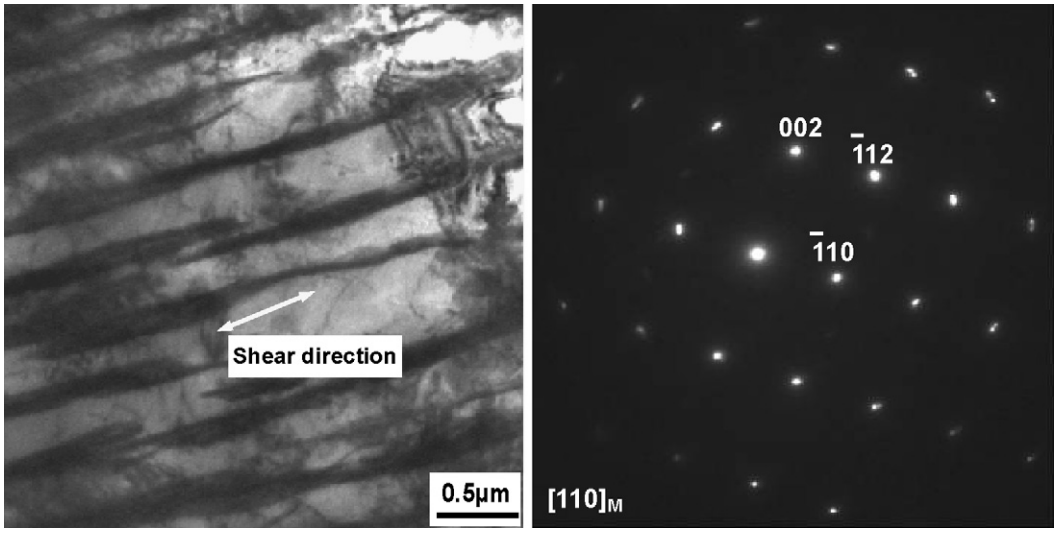

Fig. 9. TEM images of the material in the transitional zone *B* in a transformed shear band. (a) The bright field image showing the severely elongated martensite laths along the shear direction, and (b) the corresponding SAED pattern.

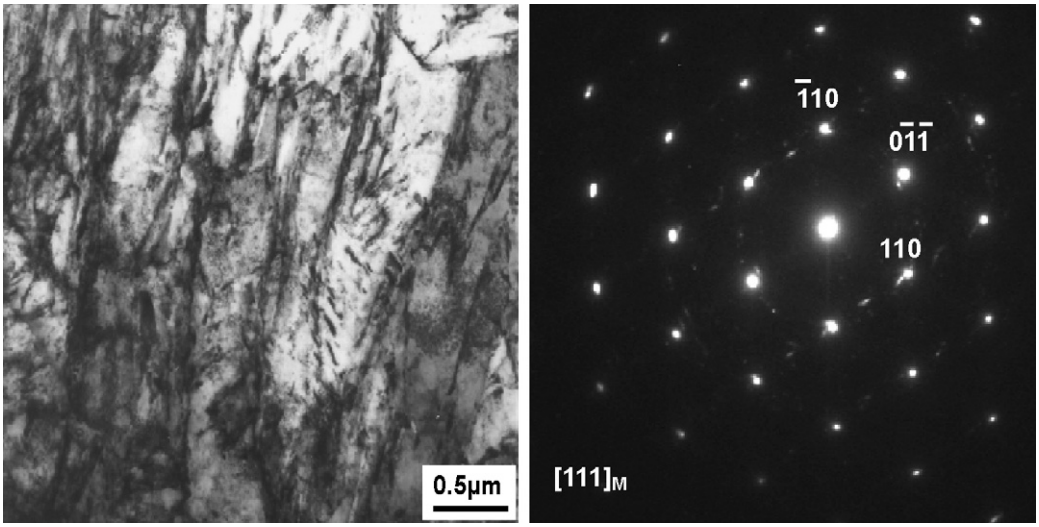

Fig. 10. TEM images of the material in the transitional zone *B* but near the center of transformed shear band. (a) The bright field image showing the martensite laths divided by dislocations, and (b) the corresponding SAED pattern.

shear direction. The dislocations are mostly at the lath boundaries. Inside the laths the dislocation density is relatively low and the slip traces are distributed homogeneously. The deformation in this zone is clearly not severe, and hence the dislocation density is not high. The diffraction pattern in Fig. 9(b) shows that the microstructure of the material in this zone is a tempered martensite structure.

On the other hand, the materials in the transitional zone adjacent to the band center of the transformed shear band contain broken and elongated martensite laths in the shear direction, as shown in Fig. 10(a). A large number of dislocation tangles exist between and inside the laths. The areas which have high dislocation densities divide the elongated laths into many smaller sub-regions. The diffraction spots are slightly elongated, as shown by Fig. 10(b), indicating that the material was subjected to a larger plastic deformation, but its crystallography structure was retained and no phase change took place because the recrystallization temperature in this zone had not been reached.

Figs. 11 and 12 display the microstructure of the material in the central zone *A* in a transformed band. The material in the area close to the transitional zone *B* contains many subgrains with a high density of dislocations. The lath morphology disappears, which is similar to the recovery structure under thermal deformation, Fig. 11(a). The diffraction pattern changes from the regular lattice to discontinuous rings, Fig. 11(b). Fig. 12 shows that the material at the center of the transformed shear band contains many equiaxed grains of 0.4–0.6 μm in diameter. The dislocation density in such grains is relatively low. These grains, however, have a high angle of misorientation, and are similar to a structure from recrystallization, although their size is smaller than that of the statically recrystallized grains, as shown in Fig. 12(a). The ring-like electron diffraction pattern with intermittent spots, Fig. 12(b), demonstrates that these grains are of polycrystalline with random orientations. The indexing of the polycrystalline diffraction rings shows that these equiaxed grains are composed of martensite and cementite without residual austenite, indicating that a phase transformation should not have occurred there.

In summary, the above observation and analysis show that there are significant differences between the microstructures in the materials in a deformed shear band and a transformed shear band, although both types of ASBs are the manifestations after localized shear. This is because their formation mechanisms are essentially different. Since the mechanism to form a deformed shear band is straightforward, i.e., via a severely localized shear, our discussion below will focus on that of the transformed shear band. A transformed ASB consists of three zones, the central zone *A* containing very fine, equiaxed grains with dislocation substructures, the transitional zone *B* composed of broken subgrains and elongated laths along the shear direction, and the slightly deformed zone *C*. In both *B* and *C*, the materials retain the original regular martensite structure.

For convenience, in the following discussion, we will call the transformed shear band a shear band or an ASB without further distinction.

3.2. Microstructural evolution

The above findings provide a good understanding of the mechanism of microstructural evolution during the formation of an ASB. From the external of an ASB to its center, the material experiences a variation of strain and strain rate. The microstructures observed in different zones indirectly reflect the microstructural evolution stages in an ASB. We can therefore propose an evolution picture, as illustrated in Fig. 13, to interpret what could have happened within an ASB during the HSM of the steel. First, when the cutting operation just begins, the tempered martensite in an originally heat treated workpiece is subjected to a high strain rate deformation. A large number of dislocations start to emit. However, due to the relative low plastic straining at this stage, the morphology of the martensite laths remains, as shown in Figs. 8 and 13(a). As the deformation proceeds, adiabatic shear is triggered and the dislocation density increases sharply. The serious plastic slips cause the reorientation and elongation of the lath structure along the shear direction, as shown in Figs. 9 and 13(b). With the enhancement of the deformation localization, the dislocations begin to climb to form the dislocation cells. In the area under a high strain rate, even at a very low temperature, the cell structure formation by dislocation climbing is very strong. The local temperature also rises rapidly. Because of this, the concentration and tangle of dislocations begin to form some areas of high and low dislocation densities and eventually give rise to sub-boundaries. These subgrain cell walls are then segmented and the elongated laths refined, as shown in Figs. 10 and 13(c). As the deformation continues, many dislocations disappear due to their climbing and merging under adiabatic temperature rise, which is a process of dynamic recovery leading to subgrains with high dislocation densities as seen in Fig. 11 and illustrated in Fig. 13(d). To coordinate further deformation

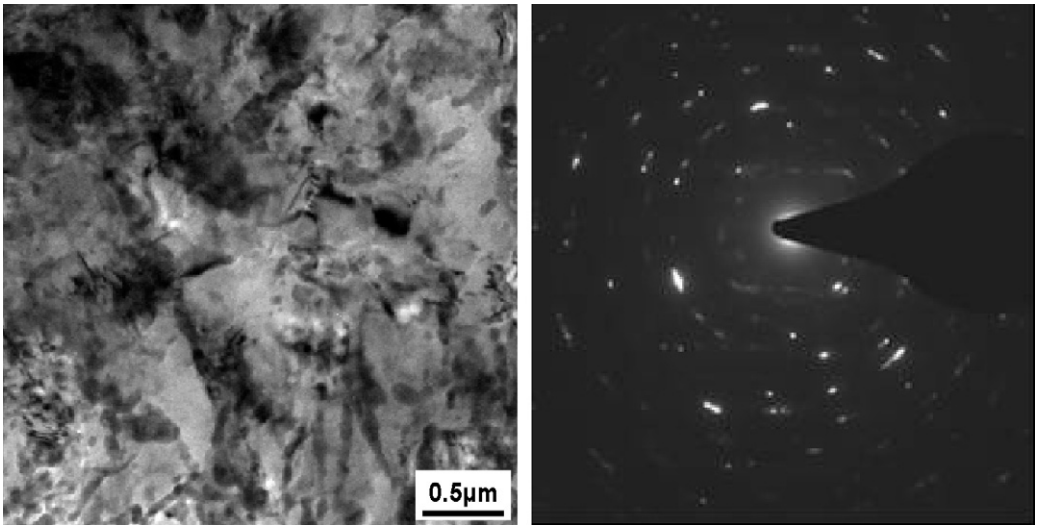

Fig. 11. TEM images of the central zone *A* close to transitional zone *B* in a transformed shear band. (a) The bright field image showing the subgrain structure, and (b) the corresponding SAED pattern.

with the increase of strain and strain rate, these refined subgrains assisted with the adiabatic temperature rise polygonally to form the equiaxed and randomly oriented recrystallized grains, as shown in Fig. 13(e). Finally, the recrystallization-induced residual stresses may introduce further dislocations to form the substructures in the equiaxed grains, as illustrated in Fig. 13(f), but the dislocation density is relatively low as revealed by Fig. 12.

In the microstructural evolution process described above, both recovery and recrystallization take place, which produces the specific microstructure of an ASB and is also the reason of material's softening leading to serrated chipping. Throughout the microstructural evolution process, the adiabatic temperature rise certainly plays an important role; but, due to the so short duration of the deformation in an HSM process, it is hard to figure out directly whether the adiabatic temperature rise has a decisive effect on the microstructural evolution, especially on the formation of equiaxed grain structure at the center of the ASBs. If the equiaxed grains are the result of recrystallization, the recrystallization mechanism is a key issue in order to clarify the microstructural formation of the ASBs. This will be discussed in the following section.

3.3. Recrystallization mechanism in ASBs

Based on the analysis above, it is reasonable to infer that the fine equiaxed grains obtained in the center of an ASB within a serrated chip are the result of recrystallization.

Temperature is one of the main factors that determine the possibility of recrystallization. In general, for a metallic material, the recrystallization temperature ranges from $0.4T_m$ to $0.5T_m$, where T_m is the melting point of the material. In the case of the workpiece material used in this study, AISI 1045 steel, $T_m = 1350\,^{\circ}\mathrm{C}$, which means that the recrystallization temperature of the material is between 540 °C and 675 °C. In order to see if this recrystallization temperature was reached or not in the ASBs of our workpiece material, let us estimate the temperature rise below.

The adiabatic temperature rise ΔT within an ASB during deformation localization can be calculated by [30]:

$$\Delta T = \frac{k\gamma\tau}{\rho c} \tag{1}$$

where τ is the average shear stress, γ is the shear strain, k is a constant ($k \cong 0.9$, i.e., about 90% of the deformation energy converted

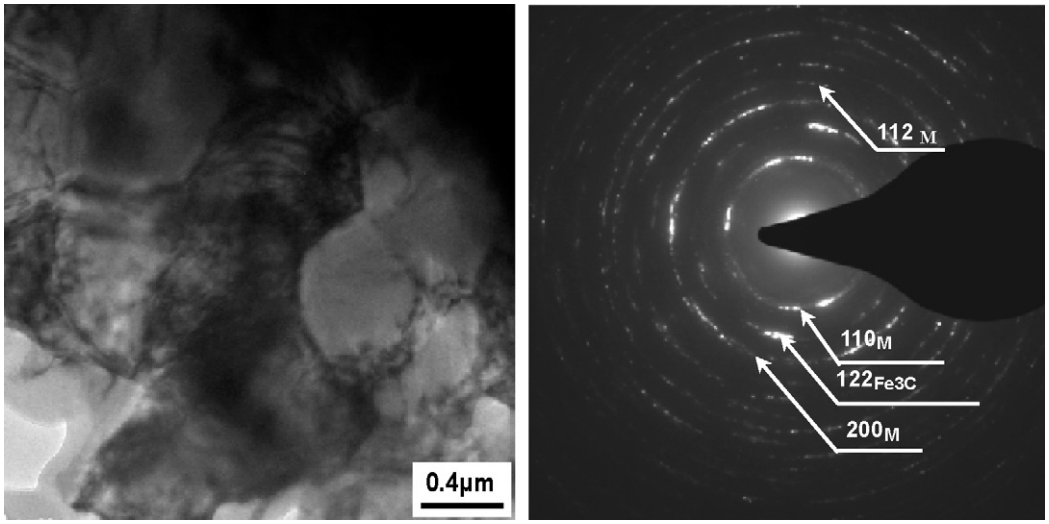

Fig. 12. TEM images of the material at the center of a transformed shear band. (a) The bright field image showing the equiaxed grains, and (b) the corresponding SAED pattern showing the polycrystalline diffraction rings.

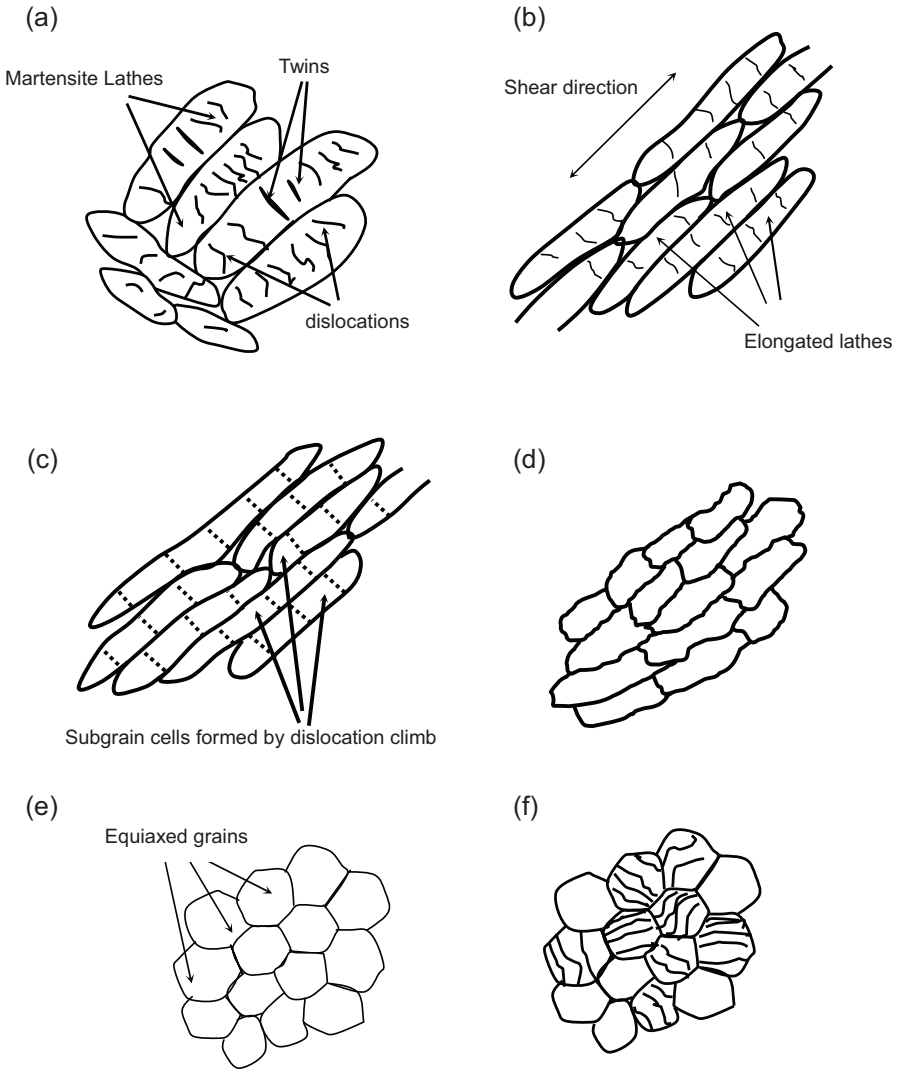

Fig. 13. An illustrative description of the microstructural evolution of the material in an ASB during the HSM of steel. (a) Initial microstructure, (b) reorientation and elongation of martensite laths along the shear direction, (c) partitioning of elongated subgrains, (d) formation of subgrains with a high density of dislocations, (e) formation of the equiaxed grain structure, and (f) formation of the substructure in equiaxed grains.

into heat), ρ and c are the material density and the heat capacity, respectively. The average shear stress in an ASB for orthogonal cutting is given by [25]:

$$\tau = \frac{\sin\ \beta \cdot [F_c \cdot \sin(\beta - \gamma_0) - F_T \cdot \cos(\beta - \gamma_0)]}{(H - (h/2)) \cdot a_w} \quad (2)$$

where F_C and F_T are the cutting and thrust forces, β is the included angle between the shear band and the bottom of the chip, γ_0 is the tool rake angle, H is the height of the chip, h is the height of the sawtooth, and a_w is the cutting width. The average shear strain in the ASB in orthogonal cutting is [25]:

$$\gamma = \frac{h \cdot \sqrt{H^2 + a_c^2 - 2H \cdot a_c \sin\ \gamma_0}}{H \cdot w \cdot \cos\ \gamma_0} \quad (3)$$

where a_c is the cutting thickness and w is the shear band width. All parameters are known or can be obtained by measurement, as shown in Fig. 14, as listed in Table 1. For the AISI 1045 steel, $\rho = 7.8 \times 10^3$ kg/m^3, $c = 474$ J/kg°C. When the cutting speed is $v = 240.3$ m/min, the calculated temperature rise within the deformed shear band is about 360 °C, which is not in the recrystallization temperature range, showing that recrystallization could not occur. This explains the reason of the formation of the deformed shear bands under this cutting speed as revealed in the previous sections. When the cutting speed increases to 432.6 m/min, the calculated temperature in the transformed band is approximately 1290 °C, which is very much beyond the recrystallization temperature range, and also exceeds the Austenitization temperature

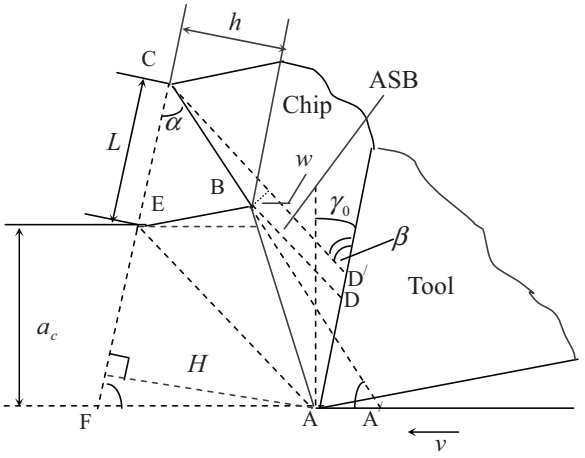

Fig. 14. A schematic diagram of serrated chip formation during orthogonal cutting.

Table 1
The measured data of a serrated chip of AISI 1045 steel.

v (m/min)	a_w (mm)	a_c (mm)	γ_0 (°)	H (mm)	h (mm)	w (mm)	β (°)	α (°)	L (mm)	F_T (N)	F_T (N)
432.6	2.5	0.15	−10	0.2	0.09	0.005	43	43	0.08	1020	1150
240.3	2.5	0.15	−10	0.18	0.07	0.030	45	44	0.15	1125	1210

(which is 727 °C for AISI 1045 steel in the equilibrium Fe–C phase diagram). However, because of the extremely short time in HSM, austenitization cannot take place. This is consistent with what we have observed above in the experiment, i.e., only recrystallization takes place.

To further confirm the accuracy of the calculated recrystallization temperature, the serrated chips with the transformed shear bands were aged at 540 °C and 560 °C for 30 min. Fig. 15 shows the change in microstructure of the transformed band at different aging temperatures. It can be seen that compared with the ASB without aging in Fig. 15(a), after the aging at 540 °C, the light-white band in the center zone became very blurred, as shown in Fig. 15(b). The ASB was widened, and the equiaxed grains could be vaguely seen but the grain size increased. This indicates that before the aging treatment, the very fine grains in the ASB were produced due to recrystallization. During the aging, these small recrystallized grains grew as the core of the secondary recrystallization, and lastly, larger recrystallized grains formed. If the recrystallization temperature of AISI 1045 steel under high strain rate loading is higher than 540 °C, the recrystallization would not occur in the deformed materials near ASB because the aging temperature did not exceed the recrystallization temperature. Only appeared the recrystallization grain growth within the center of the ASB. Therefore, in this case the ASB did not completely disappear after aging. However, after the aging treatment at 560 °C, as shown in Fig. 15(c), the recrystallized grain growth in the ASB was accompanied by nucleation. This was owing to the effect that the aging temperature was above the initial recrystallization temperature. The grains in the ASB grew and the ASB disappeared.

The above aging experiments verify that recrystallization occurred during the formation of the transformed shear bands, and that the recrystallization temperature would be in the range of 540–560 °C under the cutting speed of 432.6 m/min.

Time is another crucial factor that influences recrystallization. Recrystallization can be divided into two categories: static recrystallization and dynamic recrystallization, of which the former often occurs after deformation while latter takes place almost simultaneously with the deformation process. If the cooling rate in an ASB does not exceed the formation speed of the ASB, the recrystallization inside the ASB should be a dynamic recrystallization. The cooling rate of ASB in medium carbon steel estimated by Wittman and Meyers [31] is 10^6 kg. According to this, when the temperature rise in the ASB was 1290 °C under the cutting speed of 432.6 m/min, the time required to cool it to room temperature should be about 0.7 ms. The strain rate in the ASB during the serrated chip formation is [32]

$$\dot{\gamma} = \frac{\gamma \cdot v \cdot \cos\gamma_0 \cdot \cos(\alpha - \gamma_0)}{(L\cos\gamma_0 + a_c)\cdot \sin\alpha - H\cdot\cos(\alpha-\gamma_0)} \tag{4}$$

Thus, the formation time of the ASB is:

$$t_{\mathrm{ASB}} = \frac{(L\cos\gamma_0 + a_c)\sin\alpha - H\cdot\cos(\alpha-\gamma_0)}{v\cos\gamma_0\cdot\cos(\alpha-\gamma_0)} \tag{5}$$

where L is the spacing of the sawteeth, α is the included angle between rake tool face and free face of chip, as shown in Fig. 14. When v = 432.6 m/min, the calculated formation time of the ASB is approximately 0.09 ms, which is far less than the cooling time of the ASB. We can therefore conclude that the recrystallization in the transformed bands during HSM is a dynamic recrystallization.

Derby [33] divided the dynamic recrystallization mechanism into two types: grain boundary migration and grain rotation. The migrational dynamic recrystallization is governed by diffusion and develops by the way of nucleation and growth of recrystallization grains. This type of recrystallization is more common in metals. The rotational recrystallization does not experience the nucleation and growth processes, but is completed through the self-rotation of subgrains. This is more common in quartz, marble, salt and other geological materials. The investigation from Hine and Vecchio [17] on recrystallization kinetics in ASB of titanium and copper indicated that because the formation time of ASB is extremely short, on the order of tens of microseconds based on the strain rate of the cutting tests in this study, the migration of grain boundary is unlikely to occur in such a short period of time. Therefore, the grains of 0.6 μm observed in our experiments above should not be the result of migration of the boundaries. In other words, the recrystallization mechanism via grain boundary migration based on atomic diffusion should not be the case for the formation of the fine equiaxed grains in the ASBs here.

Meyers and Pak [34] proposed that equiaxed grains in the center of an ASB could be due to rotational dynamic recrystallization. Unfortunately, they were not able to give a good explanation. Some other researchers suggested that the grain rotation based on mechanical mechanism can well explain the formation of equiaxed grain structure within an ASB. For example, Hines et al. [17] proposed a mechanical model of subgrain rotation using the theory of crystal plasticity (see Fig. 15 of [17]), where the shear deformation starts from a single crystal. The elongated dislocation cells along the shear direction appear when the shear band has just been formed. To coordinate the deformation, the original grain is broken into subgrains. As the deformation continues, these elongated subgrains become narrower and then are refined into many equiaxed grain cells to further keep deformation balance. After this, since further deformation can no longer make grain refinement, to reach a new equilibrium the subgrains are forced to rotate, eventually leading to the formation of equiaxed grains with high angle misorientation. In this process, to help subgrain rotation, a large number of dislocations go into the sub-cell wall to avoid the grain boundary cracking. After the deformation completes, no more dislocations will move to the grain boundaries which begin to refine during cooling, leading to the final formation of the equiaxed recrystallized grains with a large number of dislocation climbing and annihilation. The above analysis shows that the rotary recrystallization is not controlled by the diffusion mechanism of nucleation and growth, but is based on a mechanical mechanism through subgrain rotation. Therefore, it is possible that the equiaxed grains with high misorientation in our HSM process were produced in a very short period of time.

Since the traditional mechanism of grain boundary migration is not able to explain the recrystallization process within an ASB, the recrystallized grain size cannot be obtained using a recrystallization kinetics equation in the form of atomic heat transfer. Under high strain rate loading, the grain size of rotational recrystallization is inversely proportional to stress level and is in line with the following relation [33]:

$$\frac{\sigma\delta}{\mu b} = K \tag{6}$$

where σ is the external stress, δ is the recrystallized grain size, μ is the elastic shear modulus, b is the burgers vector, and K is a material

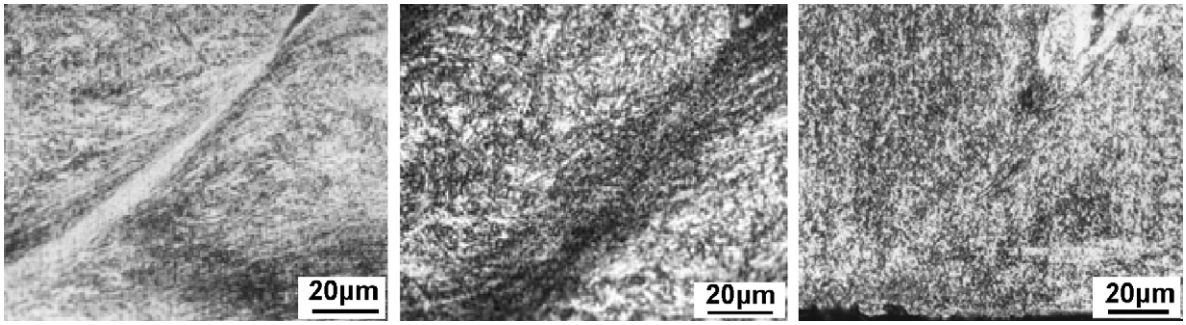

Fig. 15. Microphotographs of the adiabatic shear bands before and after aging treatments (v = 432.6 m/min). (a) Before aging, (b) after aging at 540 °C, and (c) after aging at 560 °C.

constant (for metals $K \sim 10$). This equation may be used to predict the recrystallized grain size in our ASBs induced by HSM. In the case of orthogonal cutting, σ is the average shear stress in shear zone τ. The calculated results using Eq. (2) show that for the hardened AISI 1045 steel under the cutting speed of v = 432.6 m/min and tool rake angle $\gamma_0 = -10°$, τ = 215.6 MPa. For α-Fe, the burgers vector $b = 2.48 \times 10^{-10}$ m, the elastic shear modulus of AISI 1045 steel μ = 63 GPa. Then using Eq. (6), the recrystallized grain size δ is calculated to be about 0.7 μm, which is close to 0.6 μm of the equiaxed grains observed by TEM shown in Fig. 12. This further verifies that the equiaxed grains in the center of the ASBs within the serrated chips were the products of the rotational dynamic recrystallization.

However, at a further higher or lower strain rate, a single rotary mechanism of dynamic recrystallization may be unable to fully explain the recrystallization process in ASBs. In some cases, a mixed-mode dynamic recrystallization combining rotation with migration [35] may take place.

4. Conclusions

This paper has carried out an in-depth and detailed investigation into the microstructural evolution mechanisms in the ASBs in serrated chips of hardened AISI 1045 steel produced by high speed machining. The analysis brings about the following conclusions:

(1) The HSM produced two types of ASBs, the deformed and transformed shear bands. A lower cutting speed (thus a low strain rate) leads to deformed shear bands, and a higher cutting speed (thus a high strain rate) results in transformed shear bands. The formation mechanisms of the two types of ASBs are fundamentally different. A deformed ASB is due to severe plastic shear but a transformed ASB is generated by a process of recrystallization, reorientation and elongation of the martensite laths, including partitioning of elongated subgrains, formation of subgrains and equiaxed grains by recrystallization.
(2) The dynamic rotational recrystallization is the origin of the equiaxed grains in the center of the ASBs.
(3) The martensite laths in the deformed bands were elongated along the shear direction and were broken with dense dislocations within and between the laths. The laths experienced large plastic deformation only.
(4) The microstructure inside a transformed shear band varies from the band center to the normal chip material. The transitional zone has severely elongated martensite laths with a low density of dislocations along the shear direction and with broken laths divided by the areas of high dislocation densities. The central zone consists of many subgrains with a high density of dislocations and fine equiaxed grains of 0.4–0.6 μm in diameter.

Acknowledgments

The authors would like to thank the financial support to this research from both the Chinese Natural Science Fund (No. 50875033) and the Australian Research Council.

References

[1] L. Zhen, D.L. Zou, C.Y. Xu, W.Z. Shao, Mater. Sci. Eng. A527 (2010) 5728.
[2] F. Martinez, L.E. Murr, A. Ramirez, M.I. Lopez, S.M. Gaytan, Mater. Sci. Eng. A 454–455 (2007) 581.
[3] C.G. Lee, W.J. Park, S. Lee, K.S. Shin, Metall. Mater. Trans. 29A (1998) 477.
[4] J. Krejci, J. Brezina, J. Buchar, Scripta Mater. 27 (1992) 611.
[5] J.S. Zhou, L. Zhen, Y.X. Cui, D.Z. Yang, J. Mater. Sci. Lett. 17 (1998) 391.
[6] D.H. Li, Y. Yang, T. Xua, H.G. Zheng, Q.S. Zhu, Q.M. Zhang, Mater. Sci. Eng. A 527 (2010) 3529.
[7] H.J. Yang, Y.B. Xu, J. Mater. Res. 24 (2009) 2617.
[8] Y. Yang, B.F. Wang, J. Mater. Sci. 41 (2006) 7387.
[9] Y. Yang, B.F. Wang, Mater. Lett. 60 (2006) 2198.
[10] Y. Yang, X.M. Zheng, Z.H. Li, Q.Y. Li, Acta Mater. 44 (1996) 561.
[11] P. Landau, A. Venkert, D. Rittel, Metall. Mater. Trans. 41A (2010) 389.
[12] D. Rittel, P. Landau, A. Venkert, Phys. Rev. Lett. 101 (2008) 165501–165511.
[13] Q. Xue, G.T. Gray III, Metall. Mater. Trans. 37A (2006) 2447.
[14] Q. Xue, G.T. Gray III, Metall. Mater. Trans. 37A (2006) 2435.
[15] B. Hwang, S. Lee, Y.C. Kimc, N.J. Kimb, D.H. Shin, Mater. Sci. Eng. A 441 (2006) 308.
[16] M.T. Perez-prado, J.A. Hines, K.S. Vecchio, Acta Mater. 49 (2001) 2905.
[17] J.A. Hines, K.S. Vecchio, S. Ahzi, Metall. Mater. Trans. 29A (1998) 191.
[18] Y.B. Xu, H.J. Yang, M.A. Meyers, Scripta Mater. 58 (2008) 691.
[19] H. Yan, S.W. Xu, R.S. Chen, S. Kamado, T. Honma, E.H. Han, Scripta Mater. 64 (2011) 141.
[20] M.D. Nave, M.R. Barnett, H. Beladi, ISIJ Int. 44 (2004) 1072.
[21] M.Z. Quadir, M. Ferry, O. Al-Buhamad, P.R. Munroe, Scripta Mater. 57 (2009) 29.
[22] Y.B. Xu, Y.L. Bai, M.A. Meyers, J. Mater. Sci. Technol. 22 (2006) 737.
[23] Y.B. Xu, W.L. Zhong, Y.J. Chen, L.T. Shen, Q. Liu, Y.L. Bai, M.A. Meyers, Mater. Sci. Eng. A 299 (2001) 287.
[24] Y.B. Xu, J.H. Zhang, Y.L. Bai, M.A. Meyers, Metall. Mater. Trans. 39A (2008) 811.
[25] C.Z. Duan, M.J. Wang, J. Mater. Sci. Technol. 20 (2004) 775.
[26] C.Z. Duan, M.J. Wang, J. Mater. Process. Technol. 168 (2005) 102.
[27] C.Z. Duan, L.C. Zhang, H.Y. Yu, M.J. Wang, Adv. Mater. Res. 321 (2011) 154–155.
[28] J.D. Puerta Velasquez, B. Bolle, P. Chevrier, G. Geandier, A. Tidua, Mater. Sci. Eng. A 469 (2007) 452–453.
[29] M.A. Meyers, Y.B. Xu, Q. Xue, M.T. Perez-Prado, T.R. McNelley, Acta Mater. 51 (2003) 1307.
[30] Y.L. Bai, Res. Mech. 31 (1990) 133.
[31] C.L. Wittman, M.A. Meyers, Metall. Trans. 21A (1990) 707.
[32] C.Z. Duan, M.J. Wang, J.Z. Pang, G.H. Li, J. Mater. Process. Technol. 178 (2006) 274.
[33] B. Derby, Acta Metall. Mater. 39 (1991) 955.
[34] M.A. Meyers, H.R. Pak, Acta Metall. 34 (1986) 2493.
[35] Q. Li, Y.B. Xu, Mater. Sci. Eng. A276 (2000) 250.